Journal of Cranio-Maxillo-Facial Surgery 47 (2019) 6–14

Contents lists available at ScienceDirect

Journal of Cranio-Maxillo-Facial Surgery

journal homepage: www.jcmfs.com

Evaluation of accuracy and sensory outcomes of mandibular reconstruction using computer-assisted surgical simulation☆

Zhihang Zhou [1], Haoming Zhao [1], Shanyong Zhang*, Jisi Zheng**, Chi Yang***

[a] Department of Oral and Maxillofacial Surgery, Ninth People's Hospital, Collage of Stomatology, Shanghai JiaoTong University School of Medicine, Shanghai, China

ARTICLE INFO

Article history:
Paper received 24 June 2018
Accepted 4 October 2018
Available online 11 October 2018

Keywords:
Mandibular reconstruction
Inferior alveolar neurovascular bundle (IANB)
Computer-assisted surgical simulation (CASS)
Surgical template (ST)
Postoperative standardization evaluation

ABSTRACT

Purpose: To introduce a modified protocol for mandibular reconstruction and evaluate the protocol using a standardized assessment method.
Method: This retrospective study involved a case series of nine patients who underwent mandibular reconstruction between 2015 and 2017. The modular protocol comprised three novel modifications in terms of computer-assisted surgical simulation (CASS); surgical template (ST), and surgical procedure. The standardized postoperative evaluation consisted of operation time, part comparison analysis (PCA), facial symmetry, and mechanical quantitative sensory testing.
Results: The surgery successfully removed the affected mandible and preserved the inferior alveolar neurovascular bundle (IANB). PCA revealed that the mean error and standard deviation were 0.92 and 0.96 mm, respectively, for all mandibular surface sites. Follow-up results showed good facial symmetry, existence of sensation in lower lip, and no significant differences in pulp vitality between both sides ($p = 0.181$). Also, the results showed a reduction in the overall operating time.
Conclusion: The modified mandibular reconstruction method used in this study could repair lateral mandibular defects and preserve the sensory function of the chin and lower lip.

1. Introduction

Defects of the mandible, typically caused by tumors such as ameloblastoma, ossifying fibroma, and myxoma, often lead to severe facial deformity and difficulty with chewing, which, in turn, markedly affect a patient's quality of life. Reconstruction after segmental resection of the mandible has been performed using various techniques, including iliac bone grafts (Zheng et al., 2018), fibular bone grafts (Hidalgo, 1989), costochondral grafts (Bauder et al., 2015), sliding vertical osteotomy on the posterior border of the mandibular ramus (Martinez-Lage et al., 2004), sternoclavicular grafts (Singh et al., 2012), scapular flaps (Singh et al., 2012), and vascularized second metatarsal joint grafts (Landa et al., 2003).

Traditionally, grafts from different donor regions are used separately owing to differences in their characteristics and applicability. The iliac crest, as well as fibular and rib bones, are common sources for autologous bone grafts. Given that the anterior superior iliac spine is morphologically similar to the angle of the mandible, it is the most widely used bone for reconstruction. In the past, surgeons have had to use their experience and operative skills to determine the appropriate method for performing osteotomy, as well as graft harvesting and shaping. In most cases, the inferior alveolar neurovascular bundle (IANB) could not be preserved. Occasionally, functional and cosmetic outcomes can be dissatisfactory as a result of inaccuracies in the reconstruction procedure (Cordeiro et al., 1999; Deek and Wei, 2016).

☆ This work was supported by the Shanghai Committee of Science and Technology (16441908800), Key Project of the Shanghai Municipal Health and Family Planning Commission (201640001), Shanghai Shenkang Project (16CR3104B), Medicine and Engineering Fund of Shanghai Jiao Tong University (YG2017MS04), Medicine and Engineering Youth Fund of Shanghai Jiao Tong University (YG2017QN05, YG2017QN12), Seed Fund of Shanghai Ninth People's Hospital (JYZZ019).
* Corresponding author. Department of Oral Surgery, Ninth People's Hospital, College of Stomatology, Shanghai Jiao Tong University School of Medicine, Shanghai Key Laboratory of Stomatology & Shanghai Research Institute of Stomatology, No. 639, Zhi-Zao-Ju Road, 200011, Shanghai, China. Fax: +86 021 53072423.
** Corresponding author.
*** Corresponding author.
E-mail addresses: zhangshanyong@126.com (S. Zhang), 237111641@qq.com (J. Zheng), yangchi63@hotmail.com (C. Yang).
[1] These authors contributed equally to this work.

https://doi.org/10.1016/j.jcms.2018.10.002
1010-5182/

Nowadays, advanced engineering technology, including medical image processing, computer-assisted surgical simulation (CASS), and three-dimensional (3D) model printing, is widely used in medical research, particularly in maxillofacial surgeries such as orthognathic surgery (Salmen et al., 2017), dental implants (Greenberg, 2015; Calvo Guirado et al., 2018), apicectomy (Spies et al., 2018), and mandibular reconstruction (Tarsitano et al., 2014; Ikawa et al., 2016). With such advanced techniques, surgeons can precisely diagnose the defect in a 3D environment, predesign a surgical plan, and accurately track the courses of nerves and vessels (Degerliyurt et al., 2009; Bagheri et al., 2012; Wittwer et al., 2012). With such precise preoperative assessment, the IANB can be protected throughout the procedure.

2. Materials and methods

2.1. Patients

This retrospective study evaluated nine consecutive patients (five men and four women), with an average age of 25 years (range 19–46), between November 2015 and March 2017. All patients were followed up for >6 months. All nine cases underwent high-resolution helical computed tomography (CT) scans (0.5–1.25 mm per layer) of both craniomaxillofacial and donor regions. A postoperative CT scan of each patient was obtained within 14 days after surgery using the same scanner. Preoperative and postoperative mandibular images were registered and compared with each other.

In order to ensure preservation of the IANB, we explored detailed pathophysiology and used strict definitions for common features across multiple diseases. All patients were classified after consultation, and the inclusion criteria were as follows: (i) according to preoperative imaging, computer-assisted diagnosis, and biopsy pathology, we selected patients whose soft tissues were not invaded by tumor (e.g. ameloblastoma, ossifying fibroma, and osteomyelitis) in whom the IANB was preserved; (ii) simultaneous mandibular reconstruction with bone flap; and (iii) the margin of the lesion was identified by preoperative CT, and the defect had invaded only the mandibular body and part of the ramus of the mandible such that the condyle could be preserved.

Exclusion criteria were aimed at preservation of IANB: (i) biopsy results revealed tumors that were invasive to both soft and hard tissues, such as squamous cell carcinoma, osteosarcoma, and myoblastoma; (ii) cases in which the margin of invasion included the condyle and necessitated reconstruction of the temporomandibular joint (TMJ); (iii) patients with history of tumor recurrence; and (iv) patients with history of mandibular reconstruction that required a second reconstruction surgery.

2.2. Modified procedure protocol

2.2.1. Technical procedure for computer-assisted surgical simulation (CASS)

The technical protocol was divided into three main modules: image, defect, and graft (Fig. 1).

1. CT data for the craniomaxillofacial region and the donor region were obtained, transformed using Mimics 17.0 software (Materialise Software, Leuven, Belgium), and then converted into 3D models of the maxillofacial skeleton using both automatic and manual segmentation techniques. The trajectory of the IANB, which was tracked in radiographs and CT images, was marked and reconstructed.
2. Based on the detailed pathophysiology and preoperative CT, polyplane-cutting paths for resection were designed using a safe range of tumor resection.
3. Simulated resection of the tumor and part of the mandible was performed and the defect model was obtained.
4. Simulation was carried out with the mandibular defect model, using Mimics software, in order to provide references for designing the templates for iliac crest bone osteotomy and

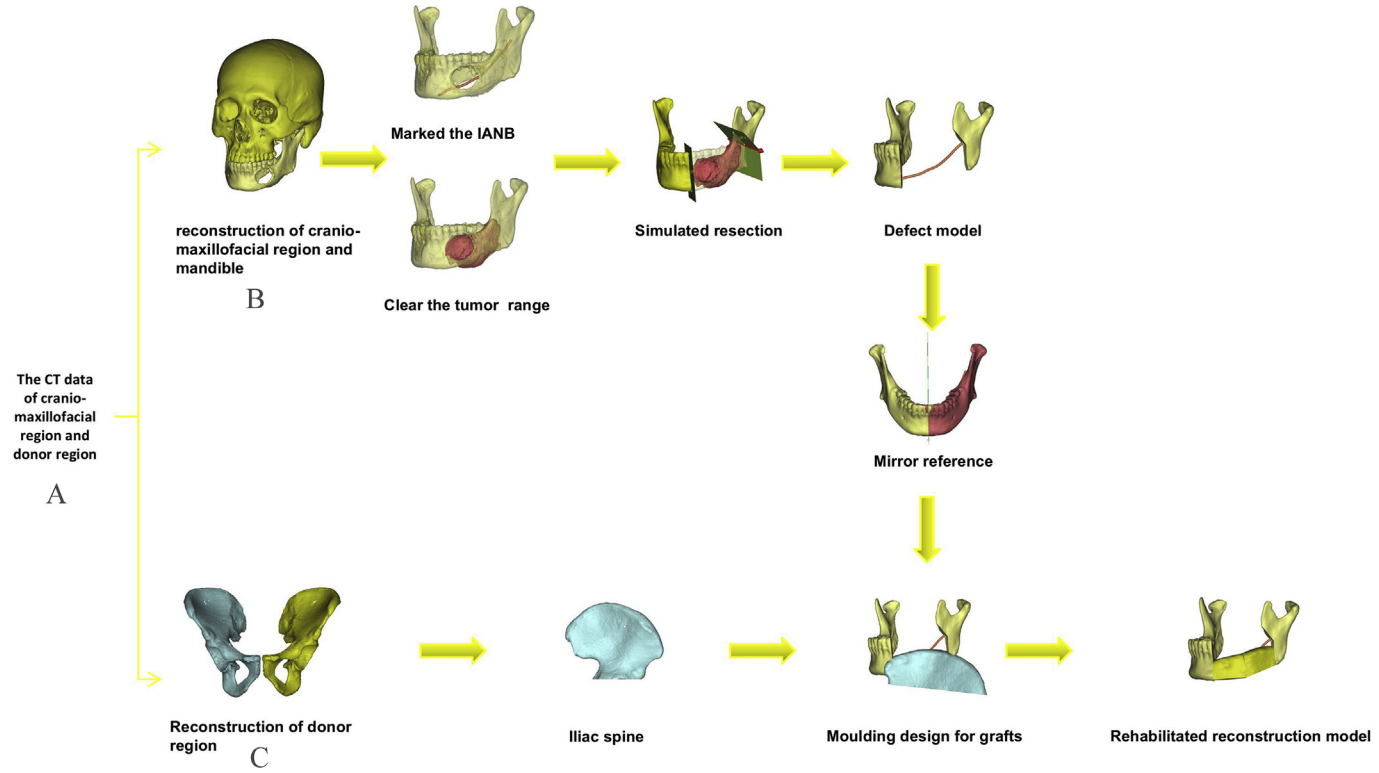

Fig. 1. Protocol for the three main modules: (A) imaging; (B) preparation of the defect; (C) preparation of the graft.

harvesting in the graft module. Based on the contralateral side, we could determine the iliac graft position under the iliac model. The graft model accurately merged with the defect model.
5. For programming surgical templates (STs), the polyplane cutting path was positioned according to the route of the IANB in order to determine the direction and depth of osteotomy.

2.2.2. Design and surgical templates (STs)

1. The CASS plan was converted into a stereolithographic (STL) file and imported into 3-matic software (research registration process; version 11.0, Materialise, NV, Leuven, Belgium).
2. To protect nerves and blood vessel, bone surface exposed during the resection could be visualized by the CASS plan.
3. The ST direction was confirmed using the CASS polyplane osteotomy cutting path.
4. The bone surface has certain morphological characteristics and smoothing it.
5. The ST model was designed by repeatedly applying amplification and Boolean mathematical operations. The section of the bony surface was designed as well.
6. Based on steps 1–5, STs for tumor resection, IANB preservation, and grafts in the region of the bone were designed using this protocol.
7. Each primary ST model was trimmed to an area less than that of the exposed bone surface and could be calibrated with an anatomical landmark.
8. The STL file of the CASS model was exported to a 3D printer (3D System Inc., USA).
9. A precurved titanium plate was inserted into the 3D skull model and scanned, which provided a reference for designing the guide plate positioning hole.
10. The Boolean mathematical operation was performed on the positioning line to produce a cylindrical shape, which was used to position the guide needle during the surgery. After fusion of the cutting line and plate-guided positioning hole, the final ST design was completed.
11. Finally, the STL file for the ST was exported to the 3D printer.

2.2.3. Preparation for surgery

1. The resection template and the guiding template in the original model were checked.
2. The iliac template was checked.
3. The titanium plate was checked to ensure consistency of the holes with the templates.
4. The length of the titanium screws was measured.
5. Plasma disinfection was carried out.

STs were calibrated using the CASS skull model, and comparisons were performed using the software to achieve two-way verification. This verification would ensure that the position of each ST was consistent with the fixed position of the titanium plate and screws. Simultaneously, the thickness of the mandible at the osteotomy site was measured using the software, and the clinician selected a suitable length for the titanium screws. Finally, the materials were sent to the operating room for disinfection (Fig. 2).

2.2.4. Surgical procedure

1. The anterior osteotomy guiding template and conservation template for IANB were positioned.
2. The posterior osteotomy guiding template was positioned.
3. Extended resection of the tumor and exposure of the IANB were carried out.
4. Guiding templates were positioned to harvest the grafts.
5. The grafts were molded to accurately fit within the defect region.
6. Vascular anastomosis of the vascularized bone flap was achieved.
7. The flap was transferred to the recipient site and fixed to the mandibular segment by means of a reconstruction plate (Fig. 3).

The procedure had to conform rigorously to the CASS virtual plan. The mandibular osteotomy was performed according to the digital template, used to mark the borders of the lesion. A careful cut was made along the upper border of the template, indicating the trajectory of the IANB, based on its depth as measured before surgery from the buccal bone surface to the canal itself. Subsequently, the IANB was separated and protected. A separated bone, with the tumor, which showed parameters almost equal to the those in the CASS plan, is shown in Fig. 4. The iliac bone was then exposed and resected as guided by the resection template, and then harvested. After the defect model was simulated together with the iliac crest, the bone was carefully cut and molded.

Tumor resection and mandibulectomy were accurately guided by templates, and the reconstruction titanium plate was fixed to the remaining mandibular segment, guided by STs according to the six marked holes that indicated the positions of the titanium screws (Fig. 5). The donor site was ipsilateral to the mandibulectomy site. The iliac crest flap was simultaneously harvested with the

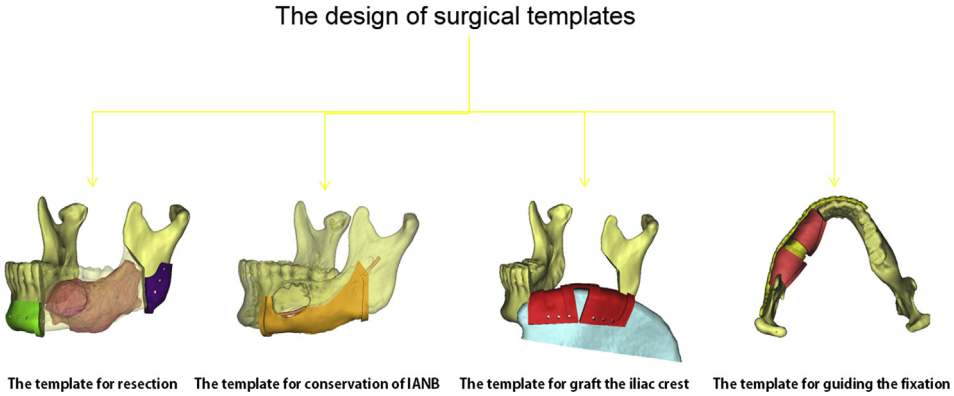

Fig. 2. Simulation with the mandibular defect model, using Mimics software, in order to provide references for designing the templates for iliac crest bone osteotomy and harvesting of the graft.

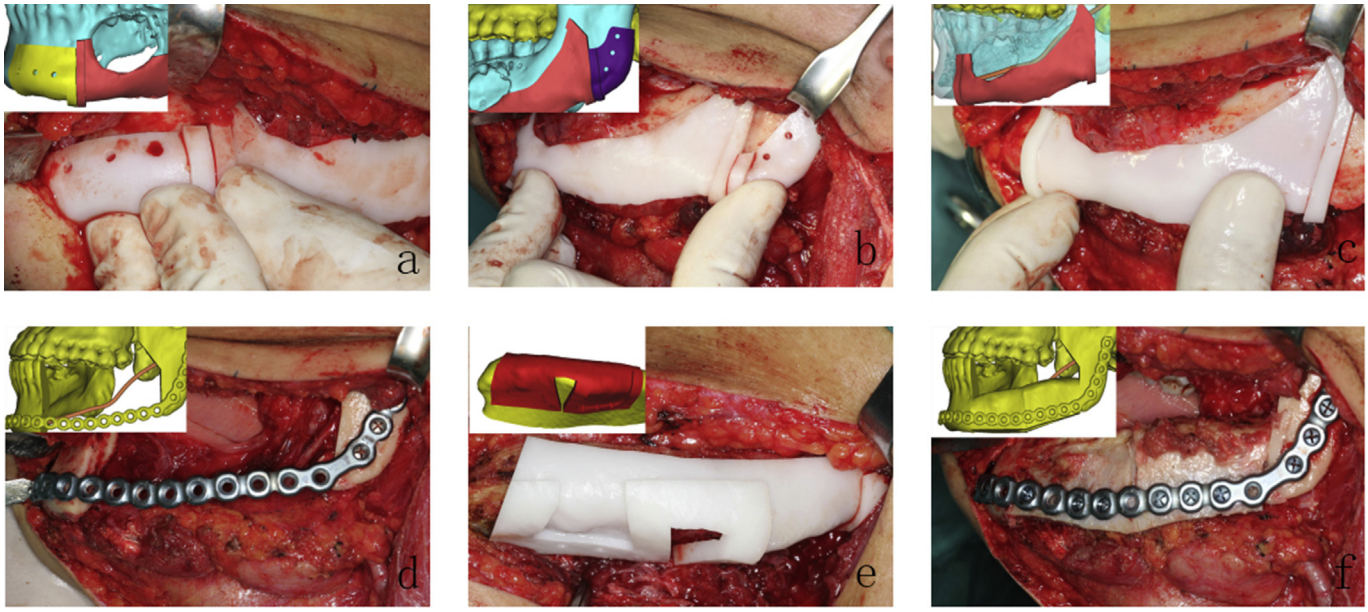

Fig. 3. Process of reconstruction surgery: (a) template for anterior osteotomy and IANB preservation; (b) template for posterior osteotomy and IANB preservation; (c) template for IANB preservation; (d) titanium plate for reconstruction and exposure of the IANB; (e) preparation of grafts; (f) completed reconstruction.

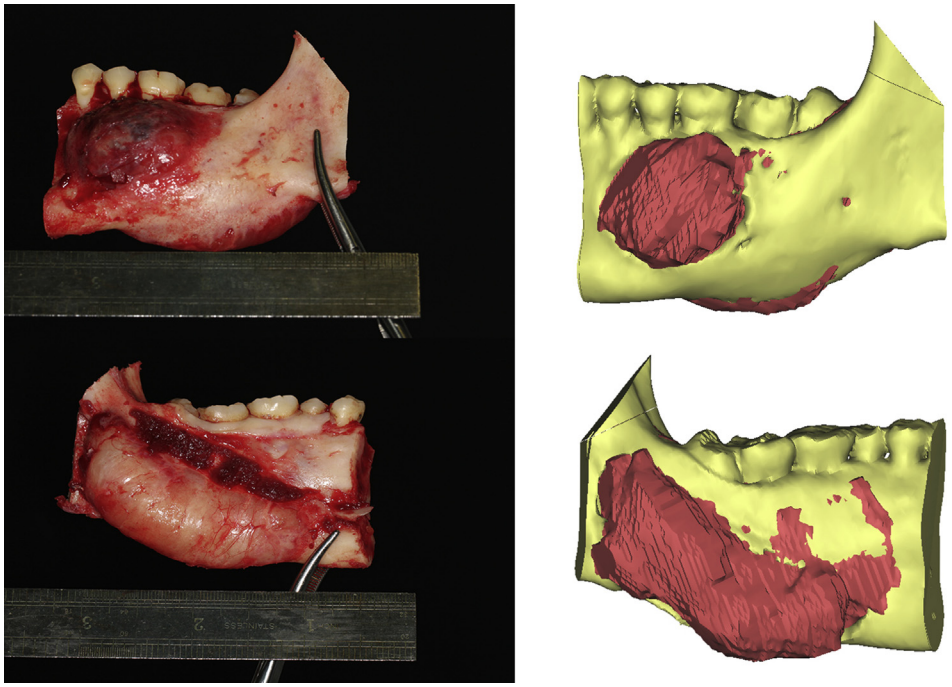

Fig. 4. Comparison of the tumor removed during surgery and the tumor reconstructed using the preoperative software.

mandibulectomy. The flap was harvested and molded using the resin model and cutting template, as mentioned earlier. The flap was transferred to the recipient site, and the pedicle was placed within a tunnel in the submandibular region to promote anastomosis. Using the navigation system, the 3D position was confirmed as matching the position in the virtual plan.

According to the predesigned CASS plan, the iliac flap was separated into two segments. The upside of the mesial segment should be similar to the occlusal surface. The distal segment was used to reconstruct the appearance and height of the mandibular angle and mandibular ramus. After intermaxillary fixation bone grafts were harvested to reconstruct the resected mandible and fixed using prefabricated plates in accordance with the model of the mirror image.

2.3. Standardized evaluation

2.3.1. Part comparison analysis (PCA)

Postoperative CT data (14 days after surgery) were imported into the Mimics 17.0 software and then converted into 3D models

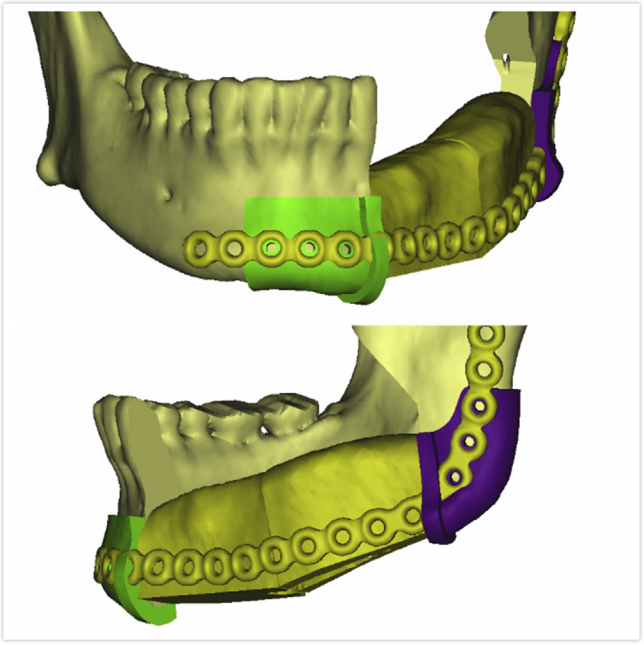

Fig. 5. Six marked holes indicating positions of the titanium screws.

of the postoperative maxillofacial skeleton, using both automatic and manual segmentation techniques. The postoperative maxillofacial skeleton was simulated using the CASS model and converted into an STL file. Finally, this STL file — the 'simulated model' — was imported into the 3-matic software. The mandibular simulated model was imported into the 3-matic software and the 'analysis' function was used to 'create part comparison analysis' (PCA). This software indicates 'mean error' and 'standard deviation' for regional error values, and allowed us to locate where the dominant error was distributed using an intuitive bar graph (Fig. 6).

'Mean error' referred to the average error value for all simulated mandibular model surface area sites, and 'standard deviation' indicated the standard deviation for these error values. PCA for facial symmetry evaluated the distance from the mandibular angle point (GoL and GoR) to the middle sagittal plane, and the distances from the condylion to the Frankfort plane and the sagittal plane (Fig. 7).

2.3.2. *Postoperative sensory evaluation of the mandible*

During the follow-up period, a Neurometer® CPT (current perception threshold) sensory detector was used to evaluate sensation in the skin of the chin and lower lip at 6 months after surgery, and the differences between the two sides were calculated to assess the function of the IANB (Fig. 8). We chose to use CPT instead of a visual analog scale/score (VAS) because CPT is the result of an objective test, whereas VAS is the result of subjective judgment. The Neurometer® CPT detector provides a numerical value between 0 and 10 depending on the nerve conduction velocity, wherein 0 indicates normal function, 10 indicates neurosensory loss, and 1–5 and 6–9 indicate neuritis and neuropathy, respectively.

3. Results

Final marginal pathology results for all nine patients were negative, confirming that all mandibular lesions had been completely removed (Table 1). Final pathology for all patients was

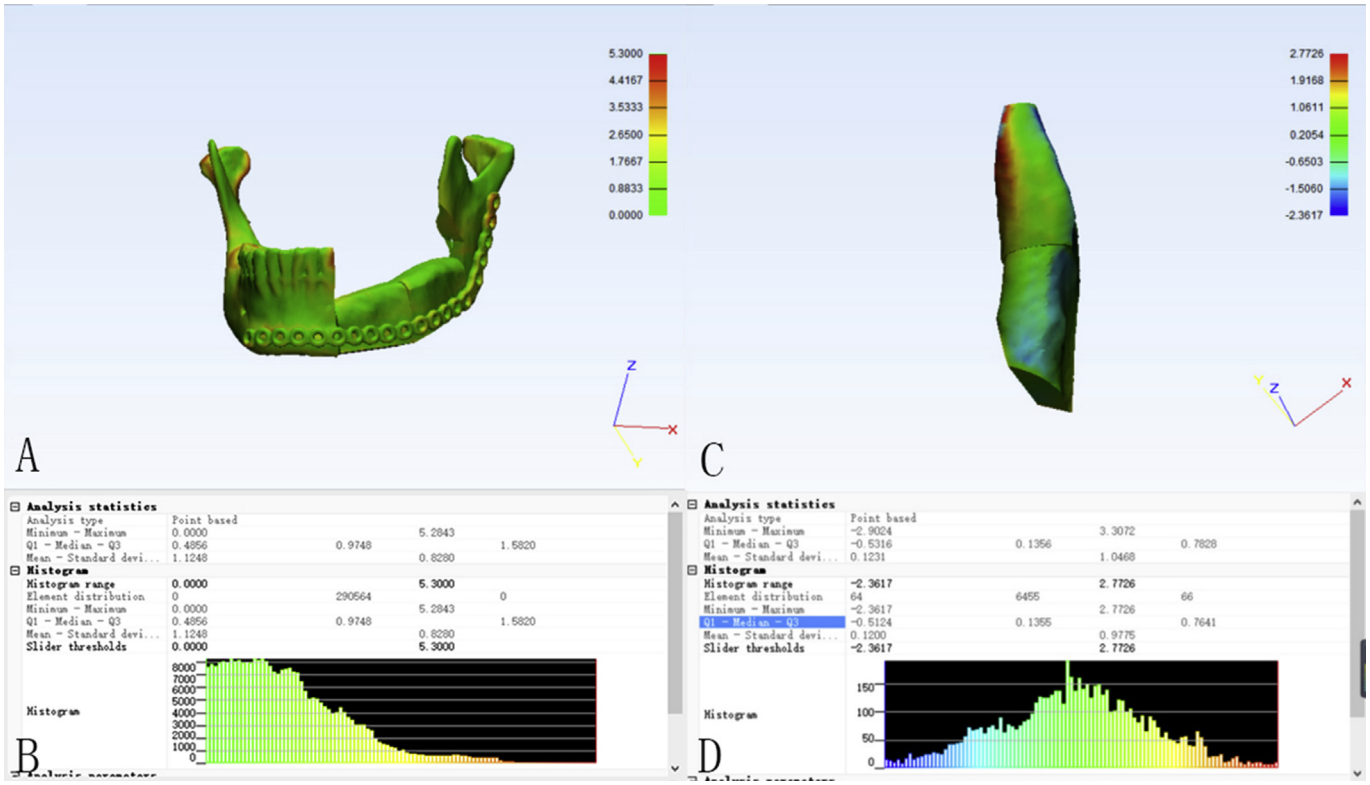

Fig. 6. Part comparison analysis (PCA): (A) error distribution throughout the mandible; (C) error distribution for the graft; (B) and (D) bar graphs showing mean error and standard deviation.

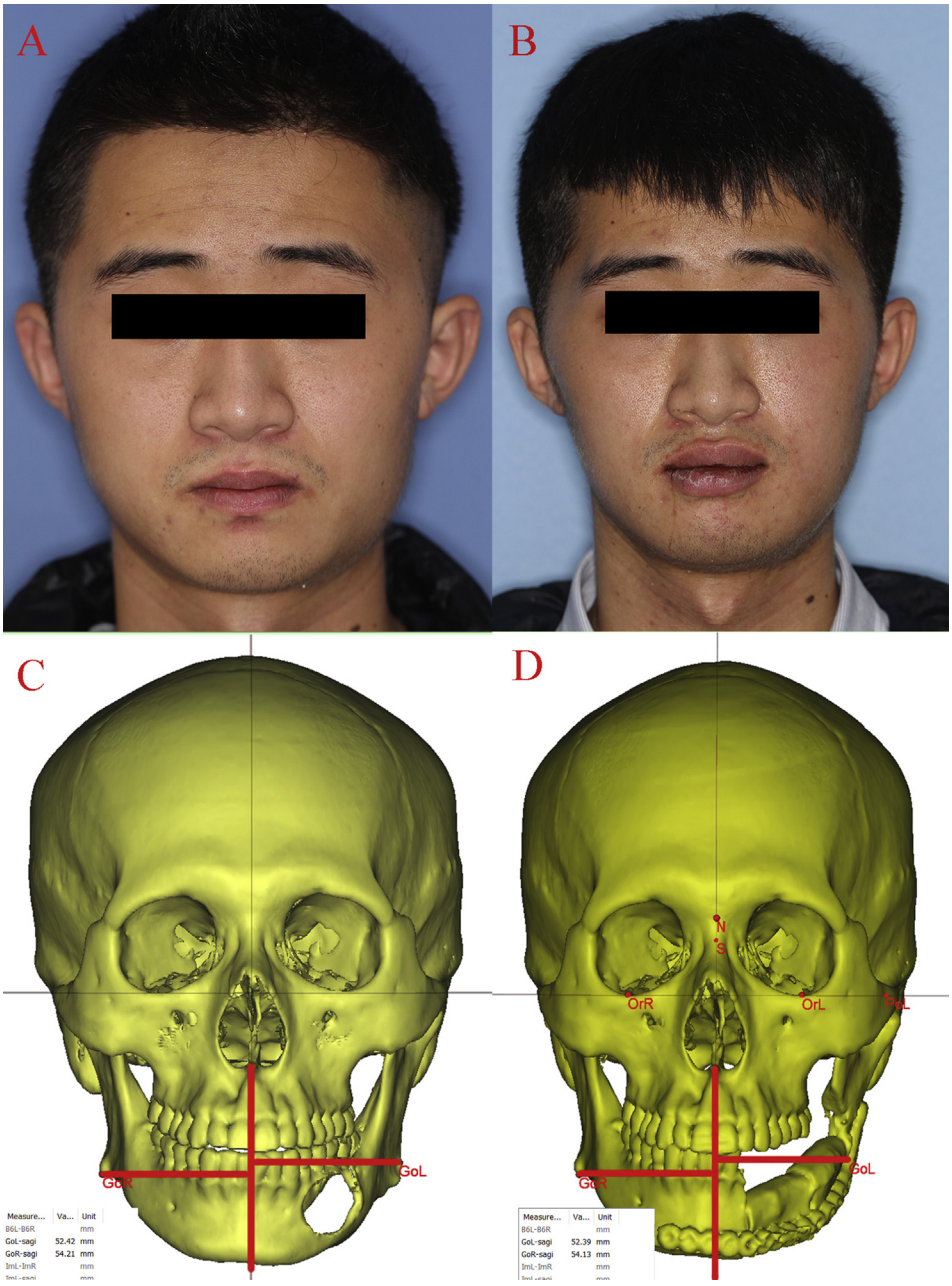

Fig. 7. (A) and (B) comparison of preoperative and postoperative patient photographs; (C) and (D) evaluation of facial symmetry.

consistent with the results of the preoperative biopsy. All patients were followed up for 6–18 months, with the optimal time for nonimmediate implant placement being 6–9 months after surgery.

Results for PCA, maximum mouth opening, and operation time are shown in Table 2. PCA results for facial symmetry are shown in Table 3. Results for the Neurometer® CPT are also shown in Table 3. The STs fitted well on the mandibular surface, and no nerve damage was found during the IANB preservation surgery. The mean error for all patients was 0.92 mm and the standard deviation was 0.96 mm. Distances from the mandibular angle point to the midsagittal plane on the reconstructed side did not differ significantly from those on the unaffected side ($p = 0.181$). Moreover, in all cases of IANB preservation surgery, CPT electrical testing revealed that sensory function of the affected side did not decrease significantly compared with the unaffected side ($p = 0.076$).

4. Discussion

CASS virtual plans and 3D printing are now widely used by surgeons in orthognathic surgery (Chin et al., 2017; Shaheen et al., 2018) and secondary maxillofacial reconstruction surgery (Schepers et al., 2016). Several researchers have tried to evaluate the accuracy of virtual surgical planning in craniomaxillofacial surgery by using different analyzing methods (Schepers et al., 2016; Weijs et al., 2016). However, the published studies lack objective postoperative evaluation, and only a few studies have focused on techniques to preserve important nerves and blood vessels. Therefore, we integrated the two technologies of PCA and Neurometer® CPT into a single postoperative evaluation system, in order to minimize subjective errors. This protocol set out the production processes to guide surgeons in designing and producing all the STs,

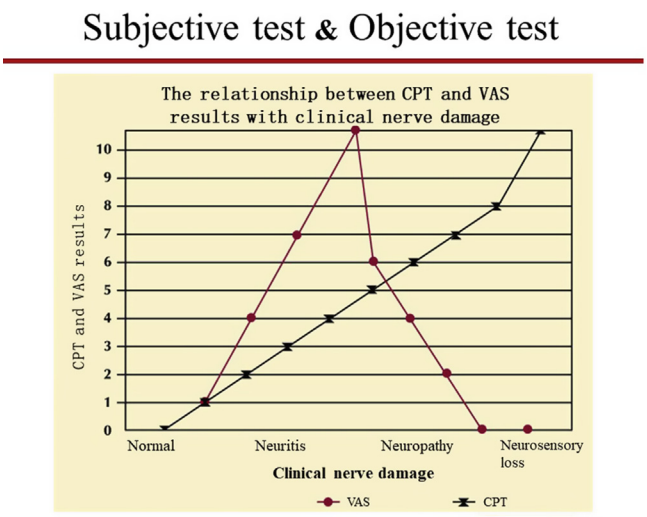

Fig. 8. Interpretation of CPT data.

including those for IANB preservation. It included several major improvements: (i) it provided 3D visualization images for diagnosis and anatomical evaluation, which, combined with preoperative biopsy results and intraoperative rapid pathology, confirmed safety margins for tumor resection; (ii) it provided accurate positioning for the IANB or other significant anatomical structures, ensuring operation safety; and (iii) it provided a postoperative quantitative evaluation method based on data from 3-matic and Neurometer® CPT.

The technique for moving from simulation to actual surgery can be addressed in two ways. One way is to use navigational surgery, which can mimic simulation results in real surgical fields by using 3D positioning rods that are fixed on the skull, face, or denture. However, the cost of this navigational approach is substantial, and precise positioning is often difficult without frequent default manipulations (Yu et al., 2016). The second option is the use of STs. STs can serve as a bridge between the CASS technology and actual surgery. Therefore, we believe that STs and CASS are complementary and mutually reinforcing, in contrast to 'experience-dependent and freehand' surgical methods. As computer simulation technologies continue to progress rapidly, they are likely to become the primary clinical and surgical tools in the future.

The first step for the CASS model was to lay a virtual plan (Foley et al., 2013; Deek and Wei, 2016; Wang et al., 2016). The entire surgical procedure was simulated in the software as 3D images. Traditional methods of reconstruction, such as CT and magnetic resonance imaging (MRI), only provide tumor, blood vessel, and soft tissue information in 2D images. Using imagination and experience to judge the 3D anatomical relationship in patients can often lead to confusion among surgeons, owing to the sophisticated anatomical structure of the oral and maxillofacial region.

The CASS procedure could not only provide clear and intuitive 3D tissue images, but these images could also be regulated by surgeons using 'movement' and 'rotate' functions. In addition, the 'reposition' function provided all angles around the target lesions as well as important anatomical structures in order to verify the adjacent relationships, which are valuable in ensuring accurate diagnosis and precise treatment. Moreover, the 3D model for the CASS plan was intuitive and easy to understand; which could also help surgeons explain surgical plans to patients and promote communication with patients and their families.

Several researchers have been in the pursuit of a completely modularized and systematic surgical plan for patients who need oral and maxillofacial defect repair surgery. The CASS-ST-PCA

Table 1
Patient characteristics.

Case	Age	Gender	Primary disease	Final pathology	Ultimate marginal pathology	Follow-up	Implant	Complications
1	21	Male	Ossifying fibroma	Ossifying fibroma	Negative	6 months	Simultaneously	Flap failure: 0
2	19	Male	Ossifying fibroma	Ossifying fibroma	Negative	18 months	6 months later	Plate exposure: 0
3	24	Male	Ameloblastoma	Ameloblastoma	Negative	9 months	Simultaneously	Plate breakage: 0
4	46	Female	Ameloblastoma	Ameloblastoma	Negative	12 months	–	Infection: 0
5	23	Male	Ossifying fibroma	Ossifying fibroma	Negative	9 months	Simultaneously	Malocclusion: 0
6	25	Female	Osteomyelitis	Osteomyelitis	Negative	18 months	7 months later	
7	24	Female	Ossifying fibroma	Ossifying fibroma	Negative	16 months	6 months later	
8	22	Male	Ossifying fibroma	Ossifying fibroma	Negative	18 months	9 months later	
9	21	Female	Osteomyelitis	Osteomyelitis	Negative	12 months	–	
Mean	25							

Table 2
Part comparison analysis (PCA) and operation time.

Case	Type of reconstruction	Postoperative assessment				
		Maximum mouth opening (mm)	Maximum deviation (mm)	Mean error (mm)	Standard deviation (mm)	Operation time (mins)
1	L + N + I + P	35	3.7	0.9	0.9	216
2	L + V + I + P	39	2.4	0.7	0.9	345
3	R + V + F + P	32	3.1	0.8	0.9	392
4	R + N + I + P	32	3.9	1	1	221
5	L + N + I + P	34	4.2	1.2	1.3	169
6	L + V + F + P	36	3.6	1.2	0.9	375
7	L + V + F + P	38	4.4	1	1.1	366
8	L + N + I + P	33	2.3	0.7	0.7	249
9	R + N + I + P	41	4.0	0.8	0.9	254
Mean		35.56	3.51	0.92	0.96	287.44

L = left, R = right; N = non-vascularized, V = vascularized; I = iliac bone graft, F = fibular bone graft; P = IANB preserved surgery.
Maximum deviation means the maximum error for whole mandibular reconstruction; mean error means the average error for all mandibular surface sites; standard deviation means the standard deviation for the error values for all mandibular surface sites.

Table 3
Mechanical quantitative sensory testing and facial symmetry.

Case (affected side)	Current perception threshold on the affected side (TG)	Current perception threshold on the normal side (TG)	Affected side mandibular angle point to midsagittal plane (mm)	Normal side mandibular angle point to midsagittal plane (mm)
1 (L + N + I + P)	7.25	6.56	52.33	45.46
2 (L + V + I + P)	7.33	7.01	47.07	46.64
3 (R + V + F + P)	0	0	48.97	48.13
4 (R + N + I + P)	0	0	46.34	47.35
5 (L + N + I + P)	0	0	55.45	55.65
6 (L + V + F + P)	7.64	7.21	44.84	45.42
7 (L + V + F + P)	0	0	50.16	49.77
8 (L + N + I + P)	0	0	46.77	45.95
9 (R + N + I + P)	8.49	7.25	43.92	40.79
p-value			$p = 0.181$	

L = left, R = right; N = non-vascularized, V = vascularized; I = iliac bone graft, F = fibular bone graft; P = IANB pre surgery.

protocol seems to meet this requirement. Moreover, beyond the CASS procedure, the virtual plan was also useful in simulating the operation as well as in detecting and handling various issues in time, for example in guiding the position and size of STs, and direction of osteotomy lines.

Surgeons were able to resolve several challenges normally encountered during surgery before general anesthesia was administered, which, in turn, greatly reduced the operation time. Accurate guiding and positioning of STs was used to improve accuracy of the operation, which included precise resection of mandibular tumors as well. The dynamic fit between the grafts and the recipient site led to avoidance of numerous molding steps for grafts, which, in turn, further reduced operation time. Moreover, accurate positioning of important anatomical structures during surgery further improved operation safety and reduced complications. Simultaneously, the IANB could be preserved in cases of benign tumors without neural invasion (Miloro and Markiewicz, 2017).

This study had certain limitations, the most important being the small sample size, and the retrospective nature of the study. In addition, simulation transfer between the CASS plan and the postoperative model could have produced subjective errors through human error during manipulation (by surgeons). However, CASS-ST surgery has certain advantages for simultaneous restoration. It can be used for secondary restoration of osteosarcomas or other malignant tumors involving hard tissues. In our future work, we also aim to use CASS-ST surgery for treatment of benign lesions of the TMJ.

5. Conclusions

The CASS-ST-PCA protocol is a systematic method that ensures accuracy of mandibular reconstruction and achieves desired results. We have simplified this protocol such that surgeons can use it to prepare a concise and efficient presurgical plan.

Conflicts of interest

None of the authors has a financial interest in any of the products, devices, or drugs mentioned in this manuscript.

Acknowledgements

We would like to acknowledge Elixigen for the English language editing of this manuscript.

Appendix A. Supplementary data

Supplementary data to this article can be found online at https://doi.org/10.1016/j.jcms.2018.10.002.

References

Bagheri SC, Meyer RA, Cho SH: Microsurgical repair of the inferior alveolar nerve: success rate and factors that adversely affect outcome. J Oral Maxillofac Surg 70: 1978, 2012
Bauder AR, Mitchell BT, Swanson J, Taylor JA, Bartlett SP: Long-term growth of costochondral rib grafts in mandibular reconstruction for craniofacial microsomia. Plast Reconstr Surg 136: 44–45, 2015
Calvo Guirado JL, Lucero-Sanchez AF, Boquete Castro A, Abboud M, Gehrke S, Fernandez Dominguez M, Delgado Ruiz RA: Peri-implant behavior of sloped shoulder dental implants used for all-on-four protocols: an histomorphometric analysis in dogs. Materials (Basel, Switzerland) 11, 2018
Chin S, Wilde F, Neuhaus M, Schramm A, Gellrich N, Rana M: Accuracy of virtual surgical planning of orthognathic surgery with aid of CAD/CAM fabricated surgical splint — a novel 3D analyzing algorithm. J Craniomaxillofac Surg 45: 1962–1970, 2017
Cordeiro PG, Disa JJ, Hidalgo DA, Hu QY: Reconstruction of the mandible with osseous free flaps: a 10-year experience with 150 consecutive patients. Plast Reconstr Surg 104: 1314–1320, 1999
Deek NF, Wei FC: Computer-assisted surgery for segmental mandibular reconstruction with the osteoseptocutaneous fibula flap: can we instigate ideological and technological reforms? Plast Reconstr Surg 137: 963–970, 2016
Degerliyurt K, Akar V, Denizci S, Yucel E: Bone lid technique with piezosurgery to preserve inferior alveolar nerve. Oral Surg Oral Med Oral Pathol Oral Radiol Endod 108: e1–e5, 2009
Foley BD, Thayer WP, Honeybrook A, McKenna S, Press S: Mandibular reconstruction using computer-aided design and computer-aided manufacturing: an analysis of surgical results. J Oral Maxillofac Surg 71: e111–e119, 2013
Greenberg AM: Digital technologies for dental implant treatment planning and guided surgery. Oral Maxillofac Surg Clin North Am 27: 319–340, 2015
Hidalgo DA: Fibula free flap: a new method of mandible reconstruction. Plast Reconstr Surg 84: 71–79, 1989
Ikawa T, Shigeta Y, Hirabayashi R, Hirai S, Hirai K, Harada N, Kawamura N, Ogawa T: Computer-assisted mandibular reconstruction using a custom-made titan mesh tray and removable denture based on the top-down treatment technique. J Prosthodont Res 60: 321–331, 2016
Landa LE, Gordon C, Dahar N, Sotereanos GC: Evaluation of long-term stability in second metatarsal reconstruction of the temporomandibular joint. J Oral Maxillofac Surg 61: 65–71, 2003
Martinez-Lage JL, Gonzalez J, Pineda A, Alvarez I: Condylar reconstruction by oblique sliding vertical-ramus osteotomy. J Craniomaxillofac Surg 32: 155–160, 2004
Miloro M, Markiewicz MR: Virtual surgical planning for inferior alveolar nerve reconstruction. J Oral Maxillofac Surg 75: 2442–2448, 2017
Salmen FS, de Oliveira TFM, Gabrielli MAC, Pereira Filho VA, Real Gabrielli MF: Sequencing of bimaxillary surgery in the correction of vertical maxillary excess: retrospective study. Int J Oral Maxillofac Surg 47(6), 2017
Schepers R, Kraeima J, Vissink A, Lahoda L, Roodenburg J, Reintsema H, Raghoebar G, Witjes M: Accuracy of secondary maxillofacial reconstruction with prefabricated fibula grafts using 3D planning and guided reconstruction. J Craniomaxillofac Surg 44: 392–399, 2016
Shaheen E, Coopman R, Jacobs R, Politis C: Optimized 3D virtually planned intermediate splints for bimaxillary orthognathic surgery: a clinical validation study in 20 patients. J Craniomaxillofac Surg 46(9), 2018
Singh V, Dhingra R, Bhagol A: Prospective analysis of temporomandibular joint reconstruction in ankylosis with sternoclavicular graft and buccal fat pad lining. J Oral Maxillofac Surg 70: 997–1006, 2012
Spies BC, Fatkulajew T, Kohal RJ, Petsch M: Contemporary digital restorative and minimal-invasive preservative surgical techniques in the esthetic zone: a case report. Implant Dent 27: 142–145, 2018
Tarsitano A, Mazzoni S, Cipriani R, Scotti R, Marchetti C, Ciocca L: The CAD-CAM technique for mandibular reconstruction: an 18 patients oncological case-series. J Craniomaxillofac Surg 42: 1460–1464, 2014
Wang YY, Fan S, Zhang HQ, Lin ZY, Ye JT, Li JS: Virtual surgical planning in precise maxillary reconstruction with vascularized fibular graft after tumor ablation. J Oral Maxillofac Surg 74: 1255–1264, 2016

Weijs W, Coppen C, Schreurs R, Vreeken R, Verhulst A, Merkx M, Bergé S, Maal T: Accuracy of virtually 3D planned resection templates in mandibular reconstruction. J Craniomaxillofac Surg 44: 1828–1832, 2016

Wittwer G, Adeyemo WL, Beinemann J, Juergens P: Evaluation of risk of injury to the inferior alveolar nerve with classical sagittal split osteotomy technique and proposed alternative surgical techniques using computer-assisted surgery. Int J Oral Maxillofac Surg 41: 79–86, 2012

Yu Y, Zhang WB, Liu XJ, Guo CB, Yu GY, Peng X: A new procedure assisted by digital techniques for secondary mandibular reconstruction with free fibula flap. J Craniofac Surg 27: 2009–2014, 2016

Zheng L, Lv X, Zhang J, Zhang J, Zhang Y, Cai Z, Liu S: Deep circumflex iliac artery perforator flap with iliac crest for oromandibular reconstruction. J Craniomaxillofac Surg 46(8), 2018